FRICTION COEFFICIENT ESTIMATION USING AN UNSCENTED KALMAN FILTER

Yunshi Zhao, Bo Liang and Simon Iwnicki

Institute of Railway Research, University of Huddersfield

Queensgate, Huddersfield, UK, HD13DH

Y.Zhao@hud.ac.uk

FRICTION COEFFICIENT ESTIMATION USING AN UNSCENTED KALMAN FILTER

Abstract

The friction coefficient between a railway wheel and rail surface is a crucial factor in maintaining high acceleration and braking performance of railway vehicles therefore monitoring this friction coefficient is important. Due to the difficulty in directly measuring the friction coefficient, the creep force or creepage, indirect methods using state observers are used more frequently. This paper presents an approach using an unscented Kalman filter to estimate the creep force and creepage and the friction coefficient from traction motor behaviours A scaled roller rig is designed and a series of experiments is carried out to evaluate the estimator performance.

Keywords: Friction estimation, Kalman filter, Traction motor

1. INTRODUCTION

Relative motion between wheel and rail leads to the tangential forces at their interface. From early studies it was observed that the behaviour of a wheelset running on the rail could not be considered as a ‘‘pure rolling’’ motion. In fact, the evidence shows the motion is characterised by a ‘‘slow’’ sliding phenomena occurring at the contact, which is described as creepage. The forces arising from creepage are therefore indicated as creep forces and it determines the acceleration and braking performance of a railway vehicle. As the friction coefficient is a key factor determining the maximum creep force, good monitoring of the friction coefficient is very important in estimating the maximum creep force and maintaining a satisfactory acceleration and braking performance.

To monitor the contact condition between the wheel and rail, direct methods which require the measurement of wheel-rail contact force and creepage are too difficult and expensive to implement in real life. Indirect methods, which rely on measurements that are easier to obtain and estimate the wheel-rail contact condition have shown their advantage and many different approaches have been proposed previously.

Methods used in estimating the wheel-rail adhesion can be classified into two categories: lateral model based and torsional model based.

The feasibility of using a Kalman filter in estimating low-adhesion conditions using vehicle lateral dynamic responses was explored in [1]. Two different Kalman filters were used in this research, the first one focused on estimating the creep coefficient directly but the result was not satisfactory; then another more complex Kalman filter was built aiming at estimating the creep force and detecting the change of creep coefficient by further analysis of the vehicle lateral responses. However, the proposed methods cannot give an accurate enough estimation neither of the creep coefficients nor the creep forces, thus the methods are only suitable when the change in the friction coefficient is large enough.

An improved method to estimate wheel-rail creep forces was proposed in [2], where a more complex dynamic model was used to build the Kalman filter. In this method the effects of friction coefficient and track irregularities on the estimation results were analysed. The results showed that the estimation was only accurate when the friction coefficient was high and the track irregularity amplitude was low.

A multi-filter method offering a more accurate estimation of the friction coefficient between the wheel and rail profile was shown in [3]. Multiple models of different friction coefficient of a single wheelset system were built to formulate the Kalman filters. This method judges the friction coefficient by comparing the root mean square of the estimating errors of these Kalman filters, but the accuracy was still not satisfactory and had the problem of having residuals too close to each other. Accuracy can be improved by increasing the number of filters but will result in an increase in computing time and still cannot avoid the problem of choosing from residuals of similar values.

Besides using the lateral model of the vehicle, there has also been research focused on the torsional/longitudinal dynamics of the vehicle.

Two algorithms were proposed in [4] to estimate the friction coefficient at the wheel-rail interface, but the estimation error was found to be large when sudden changes occurred. The EKF method was used in both of the algorithms as the longitudinal model was nonlinear.

A combination of the Luenberger observer and integrator was developed to estimate creep force and identify the skidding (sliding) phenomenon between the wheel and roller and was validated through experiments on a scaled roller-rig [5]. In the research, the sliding phenomenon was identified based on the sudden and significant change of the estimated friction force. The skidding phenomenon was then more thoroughly studied with the implementation of the 2nd order Luenberger observer [6]. The interaction between the wheel-roller slip and the

torsional oscillations of the driving system was studied using spectrum analysis, showing that the creep force was influenced by low frequency harmonics. These two studies focused only on the skidding phenomena and did not analyse the creepage or friction coefficient.
An unscented Kalman filter based estimator is proposed in this paper. The wheel-roller dynamics as well as the motor dynamics are both included in the filter. The wheel-roller creep force is calculated using the Polach formulation [7] to give a more accurate simulation than the heuristic nonlinear creep force model [8] used previously, especially in the case of large creepage. A creepage dependent friction coefficient is also introduced into the model. A 1/5 scaled roller rig has been built for this research and used to validate performance of the estimator.

2. TEST RIG DESIGN

A 1/5 scaled roller rig has been designed to simulate railway vehicle behaviour. The rig includes a bogie with two wheelsets and two pairs of rollers underneath. As this research project is focused on the traction behaviour, each of the wheelsets is powered by an AC induction motor through a pair of spur gears, as shown in Figure 1. The traction motor adopts the axle-hung arrangement [9], connected to the wheel axle by two bearing blocks. The anti-pitch arm is designed to reduce the pitch movement of the motor against the wheelset frame. 4 rubber mounts are used as the primary suspensions between the wheelset frame and the bogie frame.

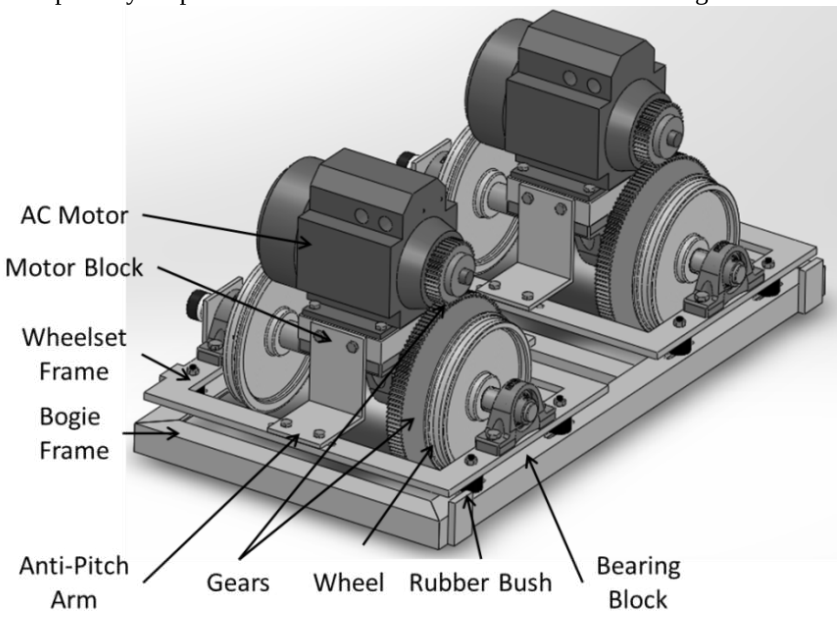

Figure 1 Bogie assembly

The roller axles are rigidly connected to the roller frame with bearing blocks at each end. The diameters of the wheel and roller are 200mm and 400mm, respectively. A large roller diameter is chosen to reduce the de-crowning effect described in [10]. The wheel profile is a 1/5 scaled UK P8 worn profile. The roller profile is a 1/5 scaled BS 113a profile with no cant.
As shown in Figure 2, two permanent magnet DC motors, which are used as generators, are connected to the roller axles and to provide traction load to the system. Rheostats are connected to the DC motors to provide various torque values. Two sets of timing belt pulleys are used to increase to the speed at the DC motor and the effective transmission ratio is 17.64.

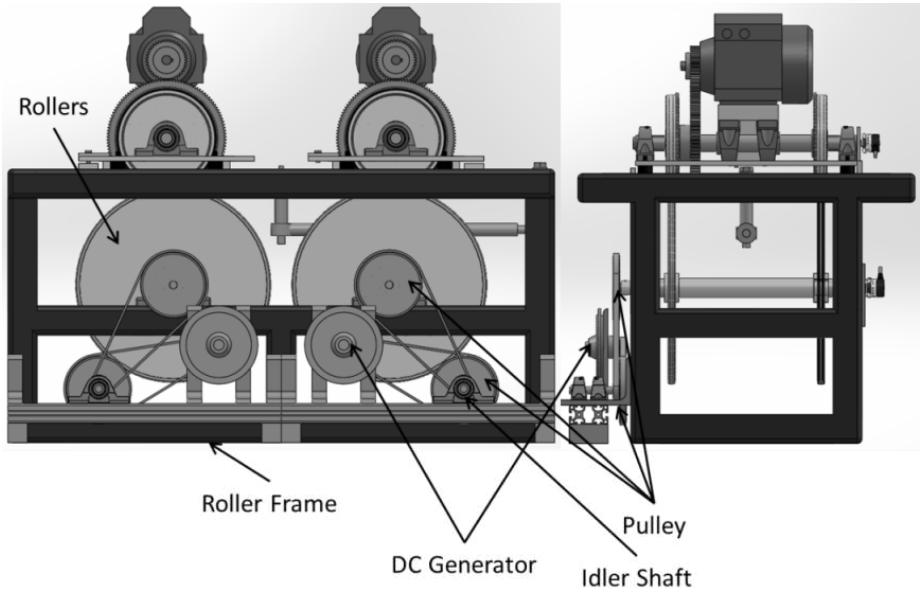

Figure 2 Roller frame design

The AC motors are powered by two inverters with an indirect field oriented control scheme [11], which is commonly used in railway vehicle traction. The stator voltage, current and speed signals of the AC motors are measured by the built in sensor of the inverter. The rotating speed of the wheel and roller are measured using incremental encoders. The output current signals of the DC generators are measured with hall-effect sensors. A Labview program is coded to process all the measured signals and give control commands to the inverters.

3. TRACTION SYSTEM MODELLING

3.1 Dynamics of the traction system

Figure 3 represents the torsional dynamic diagram of the roller rig. As the two wheelsets have no interaction when only the torsional behaviour is considered, only 1 pair of wheels and rollers is considered in the model.

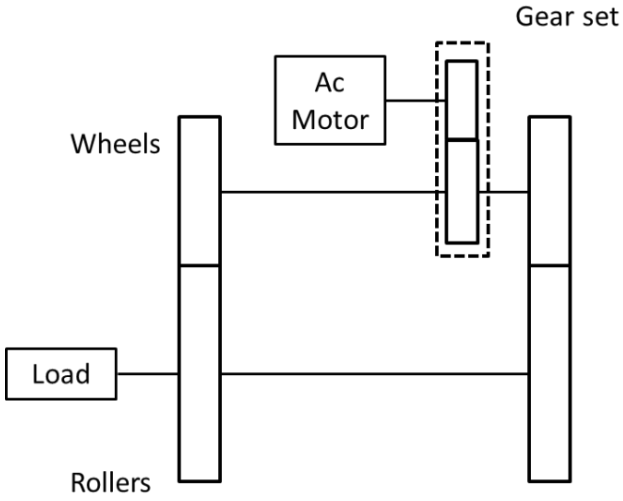

Figure 3 Block diagram of the simulated system

Hence the dynamic equations are given as:

$$\frac{d}{dt}\omega_{motor} = \frac{T_e - 2\mathrm{iR}_{\mathrm{wheel}}F_\gamma}{\mathrm{J}_{\mathrm{eqv}}} \tag{3-1}$$

$$\omega_{wheel} = \frac{\omega_{motor}}{\mathrm{i}} \tag{3-2}$$

$$\frac{d}{dt}\omega_{roller} = \frac{2\mathrm{R}_{\mathrm{roller}}F_\gamma - T_{Load}}{\mathrm{J}_{\mathrm{roller}}} \tag{3-3}$$

where $J_{eqv}=J_{motor}+J_{wheel}/i^2$, ω_{motor}, ω_{wheel} and ω_{roller} are the rotating speed of the motor, wheel and roller, J_{motor}, J_{wheel} and J_{roller}, are the rotating inertia of the motor, wheel and roller, T_e is the Electric torque of the motor. T_{Load} is the traction load applied on the roller axle. F_γ is the longitudinal creep force at the wheel – roller interface. i is the transmission ratio of the gear set.

3.2 Dynamics of the AC traction motor

The electric torque of the motor T_e is a function of the motor stator current and rotor flux components, as shown in[11]:

$$T_e = 0.75 n_p L_m (\psi_{\alpha r} I_{\beta s} - \psi_{\beta r} I_{\alpha s}) / L_r \tag{3-4}$$

While $I_{\alpha s}$, $I_{\beta s}$, $\psi_{\alpha s}$ and $\psi_{\beta s}$ can be worked out using the equations listed in Equation (3-5) to (3-8).

$$\frac{d}{dt} I_{\alpha s} = -(\frac{R_s}{\sigma L_s} + \frac{1-\sigma}{\sigma t_r}) I_{\alpha s} - \frac{L_m}{\sigma L_s L_r t_r} \psi_{\alpha r} + \frac{L_m}{\sigma L_s L_r} \omega_r \psi_{\beta r} + \frac{1}{\sigma L_s} U_{\alpha s} \tag{3-5}$$

$$\frac{d}{dt} I_{\beta s} = -(\frac{R_s}{\sigma L_s} + \frac{1-\sigma}{\sigma t_r}) I_{\beta s} - \frac{L_m}{\sigma L_s L_r} \omega_r \psi_{\alpha r} + \frac{L_m}{\sigma L_s L_r t_r} \psi_{\beta r} + \frac{1}{\sigma L_s} U_{\beta s} \tag{3-6}$$

$$\frac{d}{dt} \psi_{\alpha r} = \frac{L_m}{t_r} I_{\alpha s} - \frac{1}{t_r} \psi_{\alpha r} - \omega_r \psi_{\beta r} \tag{3-7}$$

$$\frac{d}{dt} \psi_{\beta r} = \frac{L_m}{t_r} I_{\beta s} + \omega_r \psi_{\alpha r} - \frac{1}{t_r} \psi_{\beta r} \tag{3-8}$$

where $\sigma=1-\frac{L_m^2}{L_s L_r}$ and $t_r=\frac{L_r}{R_r}$, $I_{\alpha s}$ and $I_{\beta s}$, are the stator current at α and β phase at the motor, $U_{\alpha s}$ and $U_{\beta s}$ are the stator voltage at α and β phase at the motor, $\psi_{\alpha r}$ and $\psi_{\beta r}$ are the rotor flux at α and β phase at the motor. L_s, L_r and L_m are the stator, rotor and mutual inductance of the motor. R_s and R_r are the stator and rotor resistance of the motor. n_p is the pairs of poles of the motor.

3.3 Wheel roller creep force

In this research, F_γ is modelled based on the equations developed by Polach [7, 12]. In this method, the creep force is calculated by:

$$F_\gamma = -\frac{2F_N \mu}{\pi} (\frac{k_A \varepsilon}{1+(k_A \varepsilon)^2} - \arctan(k_s \varepsilon)) \tag{3-9}$$

and for the case of the longitudinal force:

$$\varepsilon = \frac{G \pi a b C_{11}}{4 F_N \mu} \gamma \tag{3-10}$$

k_A and k_S are the reduction factors regarding to the different conditions between the wheel and rail (roller) surface. k_A is related to the area of adhesion, k_S is related to the area of slip and $k_S \le k_A \le 1$.
μ is the traction coefficient. F_N is the normal force between the wheel and roller. G is the modulus of rigidity of the wheel and roller material. a and b are the semi-axis length of the contact patch. C_{11} is the Kalker coefficient which can be found in [13]. γ is the creepage between the wheel and roller.
In this model, it is considered that the traction coefficient depends on the slip velocity V and friction coefficient, which is expressed by the following equation [12]:

$$\mu = \mu_0 ((1-D) e^{-B\gamma V} + D) \tag{3-11}$$

$$V = -0.5(R_{roller} \omega_{roller} - R_{wheel} \omega_{wheel}) \tag{3-12}$$

The creep curves with different friction coefficient are plotted in Figure 4 and the optimum creepages (γ_{opt}) which achieve maximum creep forces are also marked.

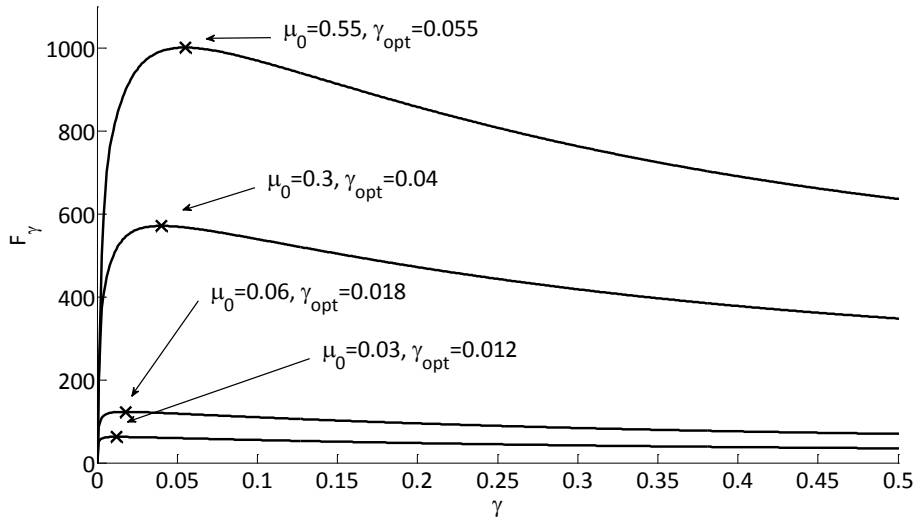

Figure 4 Creepage-creep force curves with different friction coefficients

In this simulation case, the normal force is 2kN and the forward speed is 10m/s. The values of B, D, k_A and k_S under different friction coefficient are listed in Table 1.

Table 1 Parameters of Polach model under different friction coefficients [1]

Parameter	Dry	Wet	Low	Very Low
k_A	1.00	1.00	1.00	1.00
k_S	0.40	0.40	0.40	0.40
μ_0	0.55	0.30	0.06	0.03
B	0.40	0.40	0.40	0.40
D	0.60	0.20	0.20	0.10

3.4 Dynamcis of the DC generator

The traction load is provided by the DC generator, and the load torque can be changed by varying its external resistance. The equivalent circuit of the DC generator is shown in Figure 5, where R_a is the armature resistance and R_L is the load resistance. E_a is the generated back emf (electromotive force). ω_{dc} is the rotating speed of the DC generator.

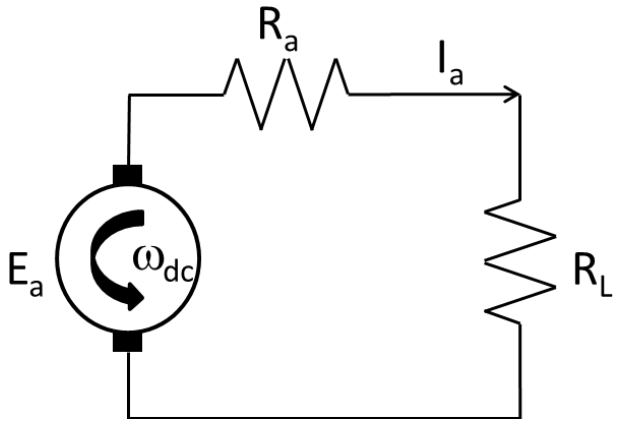

Figure 5 Equivalent circuit of the Permanent Magnet DC Generator

The following equations are used to model the DC generator:

$$E_a = k_\phi \omega_{dc} \tag{3-13}$$

$$I_a = \frac{E_a}{R_a + R_L} \tag{3-14}$$

$$T_{dc} = k_\phi I_a = k_\phi \frac{E_a}{R_a + R_L} = \frac{k_\phi^2}{R_a + R_L}\omega_{dc} \tag{3-15}$$

where k_ϕ is the magnetic constant of the DC generator.

Considering the pulley belt transmission between the DC generator and the roller axle, $T_{Load}=17.64T_{dc}$.

4. STATE OBSERVER

A general scheme of a Kalman filter based estimation system is shown in Figure 6. The Kalman filter is constructed based on the dynamic relationship which describes the monitored system and estimates state variables of the monitored system using its inputs and measurements.

For nonlinear systems, the extended Kalman filter (EKF) is one of the most popular methods. It linearizes the estimated system with Taylor expansion, which is simple and fast but can also introduce large errors when the system is highly nonlinear. To proceed accurate estimation of the highly nonlinear systems, the unscented Kalman filter (UKF) was first proposed by Julier et al in [14], and has shown its advantage over EKF[15, 16].

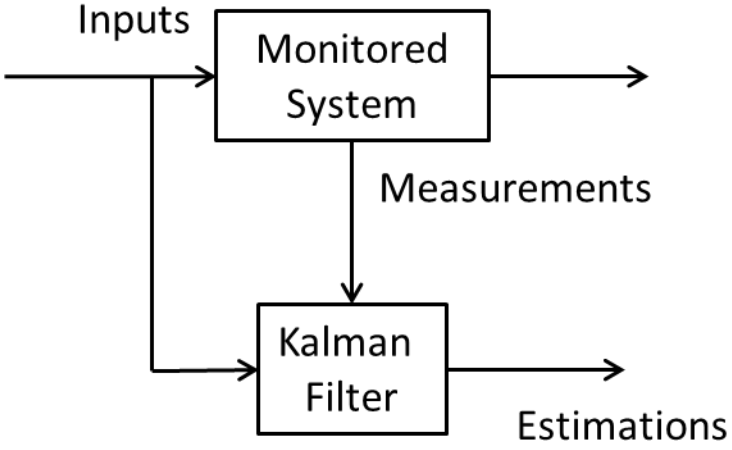

Figure 6. Block diagram for the system estimation using Kalman filter.

The performances of using EKF and UKF to monitor AC motors are compared in [17] To improve the estimation results, an unscented Kalman filter is then proposed, which avoids any linearization by utilizing a deterministic sampling approach (the unscented transformation) to calculating the state predictions and covariances. In the unscented transformation (UT), a series of sigma points are chosen based on a square root decomposition of the prior covariance, then these points are propagated through the true nonlinearity of the system, which generates the weighted mean and covariance. The differences between EKF and UKF are shown in Figure 7.

The UT calculates the statistics of a random variable which undergoes a nonlinear transformation. In the case that the state variables $\boldsymbol{x}$ (dimension p) has mean $\bar{x}$ and covariance P_x and a set of sigma points $\boldsymbol{\Sigma}$, whose associate weights $\boldsymbol{\Sigma}$=[i=0,1,…, p: $\boldsymbol{x}^{(i)}$, $W^{(i)}$] are taken. The weights $W^{(i)}$ must follow the condition [15]:

$$\sum_{i=0}^{2p} \mathbf{W}^{(i)} = 1 \tag{4-1}$$

Given these sigma points, statistics of $\boldsymbol{z}$ can be calculated. First a matrix $\boldsymbol{\chi}$ of 2p+1 sigma vectors $\boldsymbol{\chi}_i$ is formed according to the following equations [16].

$$\mathbf{X}_0 = \bar{x} \tag{4-2}$$

$$\mathbf{X}_i = \bar{x} + (\sqrt{(p+\lambda)P_x})_i, \; i = 1,...., p \tag{4-3}$$

$$\mathbf{X}_i = \bar{x} - (\sqrt{(p+\lambda)P_x})_i, \; i = p+1,...., 2p \tag{4-4}$$

$$\mathbf{W}_m^{(0)} = \lambda / (p+\lambda) \tag{4-5}$$

$$\mathbf{W}_m^{(0)} = \lambda / (p+\lambda) + (1-\alpha^2+\beta) \tag{4-6}$$

$$\mathbf{W}_c^{(i)} = \mathbf{W}_m^{(i)} = 1/2(p+\lambda) \tag{4-7}$$

where $\lambda=\alpha^2(p+\kappa)-p$ is a scaling parameter. α determines the spread of the sigma points around $\bar{x}$ and is usually set to a small positive value (e.g., le-3). κ is a secondary scaling parameter which is usually set to 0, and β is used to incorporate prior knowledge of the distribution of $\boldsymbol{x}$ (for Gaussian distributions, β=2 is optimal). $(\sqrt{(p+\lambda)P_x})_i$ is the i_{th} row of the matrix square root.

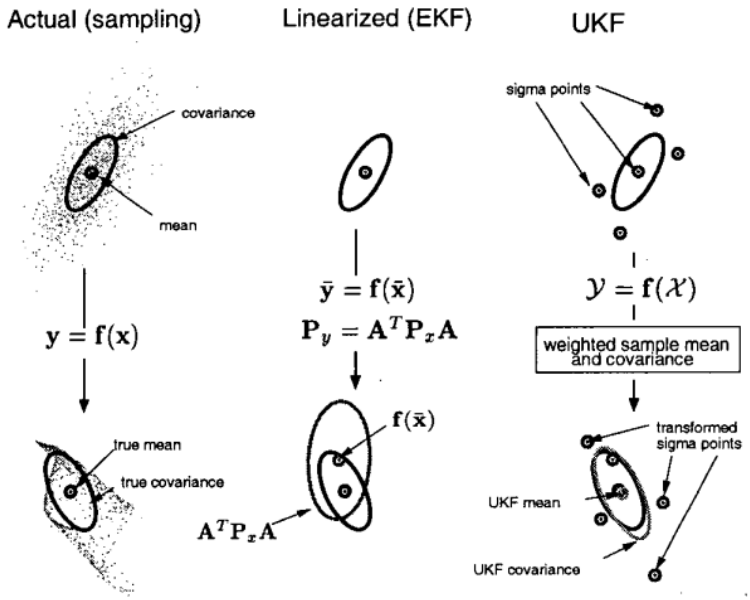

Figure 7 Comparison between UKF and EKF [18]

These sigma vectors are propagated through the nonlinear function:

$$\mathsf{Z}_i = g(\mathsf{X}_m^{(i)}),\ i = 1,....,2p \tag{4-8}$$

The mean and covariance for ***z*** are approximated using a weighted sample mean and covariance of the posterior sigma points:

$$\bar{z} = \sum_{i=0}^{2p} \mathsf{W}_m^{(i)} \mathsf{Z}_i \tag{4-9}$$

$$P_z = \sum_{i=0}^{2p} \mathsf{W}_c^{(i)} \{\mathsf{Z}_i - \bar{z}\}\{\mathsf{Z}_i - \bar{z}\}^T \tag{4-10}$$

The cross covariance matrix is:

$$P_{x_k z_k} = \sum_{i=0}^{2p} \mathsf{W}_c^{(i)} (\mathsf{X}_{i,k|k-1} - \hat{x}_k^-)(\mathsf{Z}_{i,k|k-1} - \hat{z}_k^-)^T \tag{4-11}$$

Then the normal Kalman filter algorithm can be applied as follows [18]:

$$\hat{x}_{k+1}^- = \sum_{i=0}^{2p} \mathsf{W}_i^{(m)} \mathsf{X}_{k|k-1} \tag{4-12}$$

$$P_k^- = \sum_{i=0}^{2p} \mathsf{W}_c^{(i)} (\mathsf{X}_{i,k|k-1} - \hat{x}_k^-)(\mathsf{X}_{i,k|k-1} - \hat{x}_k^-)^T \tag{4-13}$$

$$K_k = P_{x_k z_k} P_{y_k}^{-1} \tag{4-14}$$

$$\hat{x}_k = \hat{x}_k^- \quad K_k (z_k \quad \hat{z}_k^-) \tag{4-15}$$

$$P_k = P_k^- - K_k P_{z_k} K_k^T \tag{4-16}$$

For the simulated roller rig system, the state equation and measurement equation are given as:
Need some more consideration in the equationsssssss

5. EVALUATION OF THE ESTIMATOR

5.1. Overview of the estimator system

The blocks from Figure 6 can be further specified to suit the design of the estimator for the roller rig, in which case the monitored system is the roller rig and the estimator is the unscented Kalman filter. The inputs of the roller rig are the voltage and current of the traction motor; the measurements are the speed of the wheel and roller, as well as the output current of the DC generator. With all the inputs and measurements, the creep force and friction coefficient at the wheel-roller surface can then be estimated.

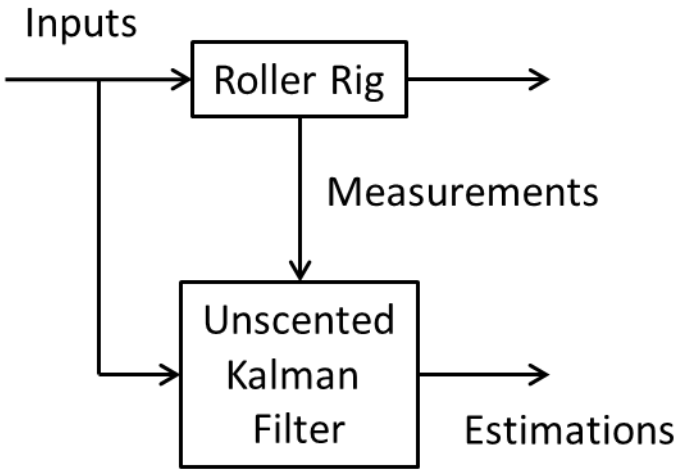

Figure 8. Block diagram for the system estimation using Kalman filter.

To summarize, the unscented Kalman filter is configured as:

$$\boldsymbol{x}_{k+1} = \mathbf{A}\boldsymbol{x}_k + \boldsymbol{w}_k \tag{4-1}$$

$$\boldsymbol{z}_k = \mathbf{H}\boldsymbol{x}_k + \boldsymbol{v}_k \tag{4-2}$$

where the state and measurement variables are:

$$\boldsymbol{x} = \left[I_{\alpha s}, I_{\beta s}, \psi_{\alpha r}, \psi_{\beta r}, \omega_{motor}, U_{\alpha s}, U_{\beta s}, \gamma, F_{\gamma}, \omega_{roller}, \mu, \mu_0, I_{dc} \right]^T \tag{5-3}$$

$$\mathbf{z} = \left[I_{\alpha s}, I_{\beta s}, \omega_{motor}, U_{\alpha s}, U_{\beta s}, \omega_{roller}, I_{dc} \right]^T \tag{5-4}$$

The system and measurement noise w_k and v_k are chosen as:

- w_k=[1e-3,1e-3,1e-3,1e-3,1e-3,1e-3,1e-3,1e-1,1e-1,1e-1,1e-1,1e-1,1e-3]
- v_k=[1e-2,1e-2,1e-2,1e-2,1e-2,1e-2,1e-2]

where the state matrix A and measurement matrix H are determined by system dynamic equations (3-1) to (3-16). As the dynamic equations are nonlinear, both A and H are worked out using numerical methods.

5.2. Estimation results

In the experiment, the two motors are given the same speed command as shown in (5-1). The motor speed command ω_{motor}^* changes every 5 seconds from 20 rad/s to 30 rad/s to create higher creepage.

$$\omega_{motor}^{*}\,(\text{rad/s}) = \begin{cases} 20 & t < 5\text{s} \\ 30 & 5\text{s} \le t < 10\text{s} \\ 20 & 10\text{s} \le t < 15\text{s} \\ 30 & 15\text{s} \le t < 20\text{s} \\ 20 & 20\text{s} \le t < 25\text{s} \\ 30 & 25\text{s} \le t < 30\text{s} \\ 20 & 30s \le t \end{cases} \tag{5-5}$$

First the base condition with no contaminants between the wheel and roller surfaces is tested and the estimations of the creep force, creepage and friction coefficient are shown in Figure 8. In case 0, the DC generator is not connected and the external resistance of the generator decreases from case 1 to case4. The resistance values for each case are listed in Table 2.

Table 2 Load resistance values of the DC generator

	Base	Water	Oil
Case 0	Infinite	Infinite	Infinite
Case 1	3Ω	4.5Ω	7Ω
Case 2	1.5Ω	3Ω	4.5Ω
Case 3	1Ω	1.5Ω	3Ω
Case 4	0Ω	1Ω	1.5Ω

The difference in the traction load can be found in the plot (a), the output current of the DC generator decreases with the resistance. For each load case, I_{dc} follows the changes of the roller speed as indicated in equation (3-16).

The creepage and creep force estimations in plot (b) and (c) also show that the creepage and creep force also increase while the traction load is larger.

The friction coefficient estimation in plot (d) shows that the result for case 0 is very low and cannot be true when the wheel and roller surfaces are dry. This estimation error is possibly caused by the fact that the traction load is negligible in case 0, as shown in plot (a), thus the effect of friction coefficient on the creep force is not significant. Therefore the estimator is not reliable when there is no traction load.

For case 1 to 4 the estimated μ_0 oscillates around 0.28, which is reasonable for the experiment case. However, in cases 1 to 3, the oscillations of the estimated μ_0 are quite significant and have a similar frequency to the creepage and creep force results. When the creepage increases to a much larger value in case 4, the estimated μ_0 is much more stable.

Therefore, the results in Figure 8 prove that the estimator is able to provide acceptable performance under enough traction load and the estimation error reduces while the traction load increases.

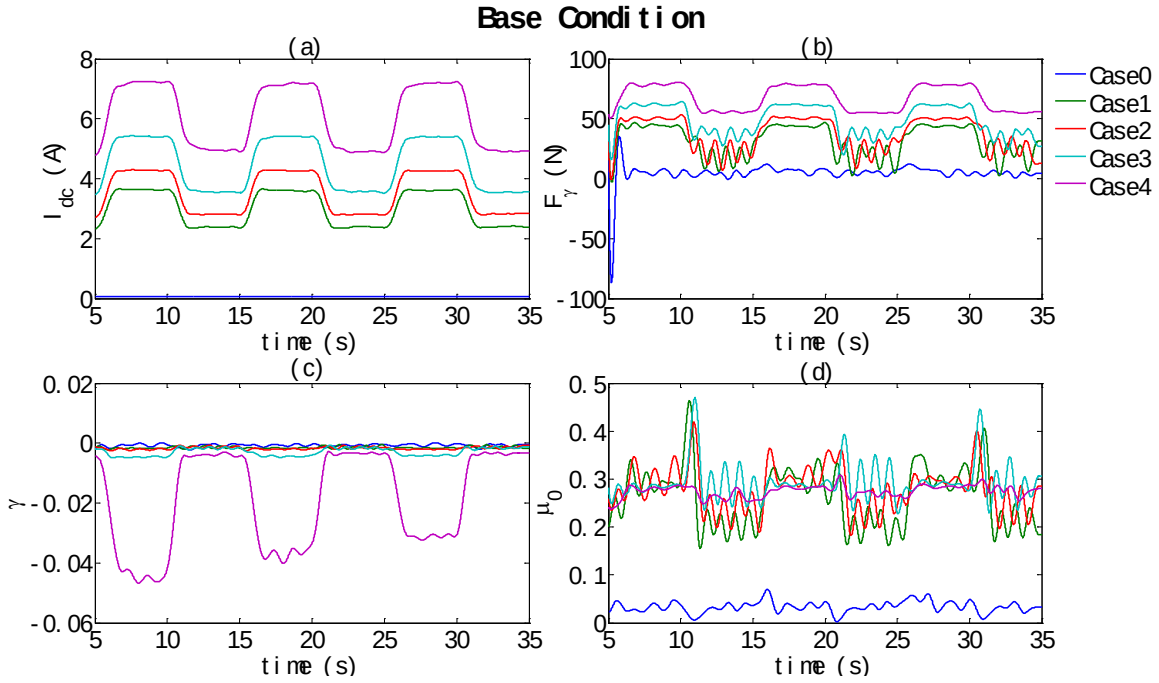

Figure 9 Estimation result for the base condition

The performance of the estimator under water and oil contamination has been studied. Water was sprayed evenly onto the wheel and roller surfaces and 5 tests with different DC generator external resistances as listed in Table 2 are carried out. Then the wheel and roller surfaces are cleaned and tried thoroughly before oil was sprayed onto the wheel and roller surfaces and repeat the same tests as in the base and water contamination conditions.

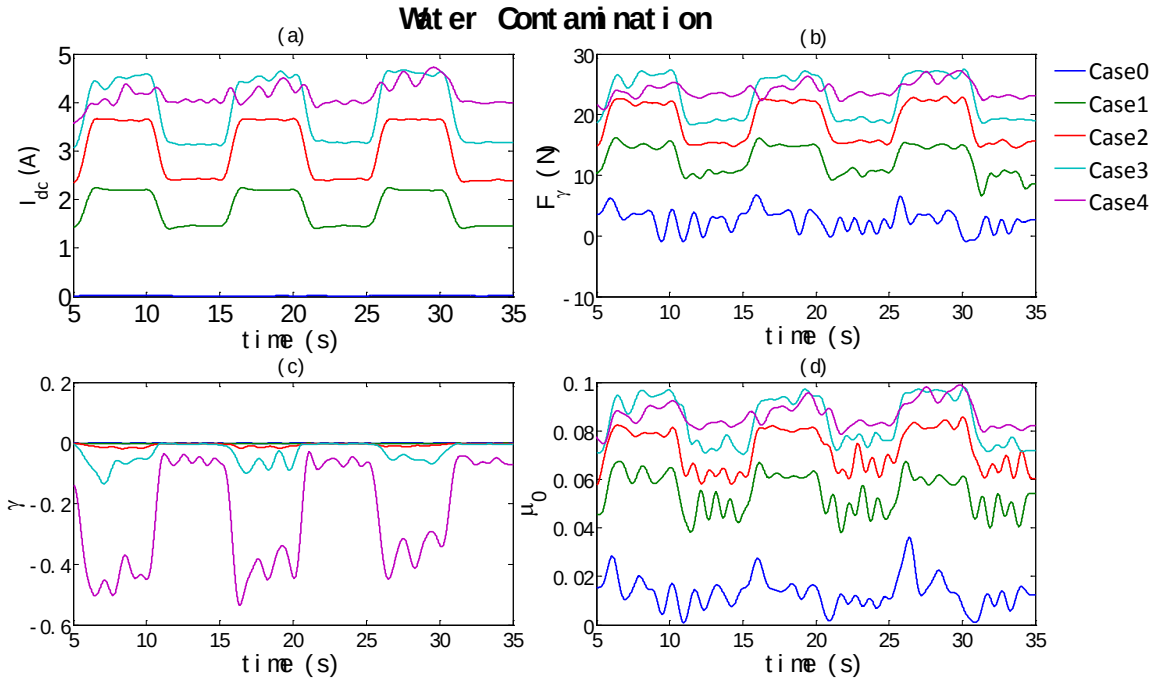

Figure 10 Estimation results for the water contamination condition

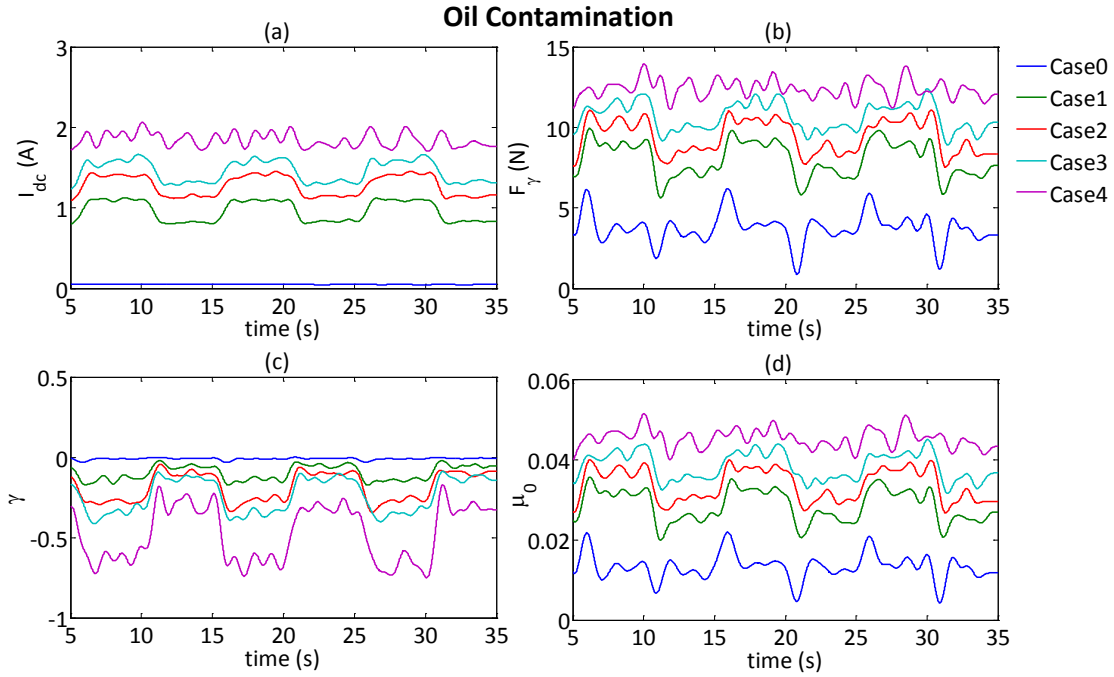

Figure 11 Estimation results for the oil contamination condition

Figure 9 and Figure 10 show the output values of the UKF under water and oil contamination respectively. In plot (a) of Figure 9 and Figure 10, I_{dc} increases from case 0 to case 3. In case 4, the wheel and roller reaches full slip thus the roller speed does not increases with the AC motor speed, which explains why the pattern of I_{dc} for case 4 is different from those of other cases.

In plot (d) of Figure 9 and Figure 10, it is clear that the estimated μ_0 values for each case have the same pattern as the creep force, which means that a higher traction load will result in a higher friction estimation. This trend is also seen in Figure 11, which plots the average values of the estimated μ_0 for all the tested cases. This problem is most possibly because that the friction coefficient is very sensitive to the sensor resolution and sample frequency. The inaccuracy of the creep force model can also lead to estimation errors as well. The noise matrices for the system and measurements are also very important to retain the estimator reliability.

Despite the estimation errors discussed above, the average μ_0 estimation under water and oil contaminations still remains around 0.08 and 0.04, respectively.

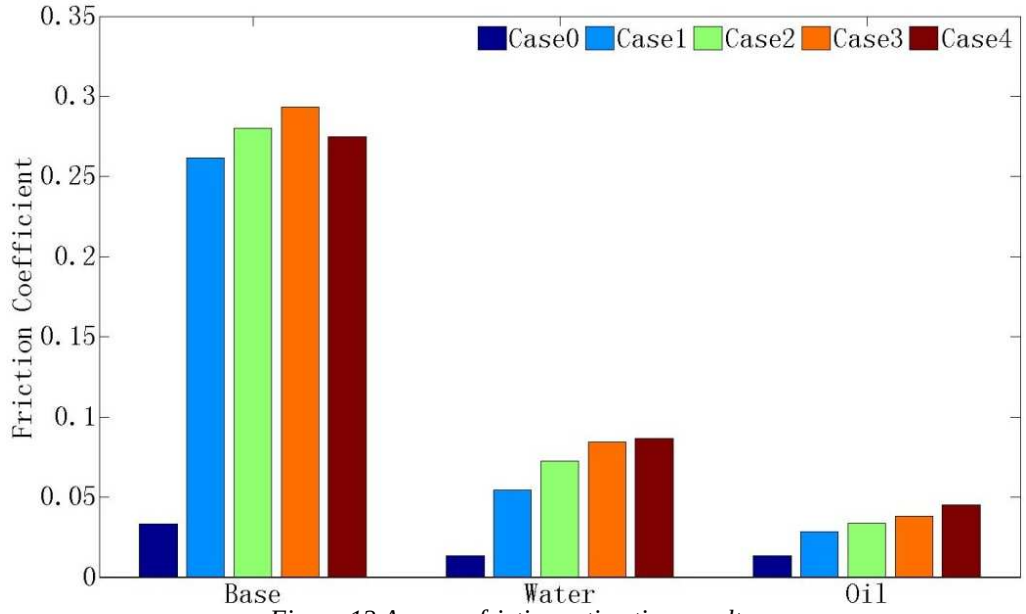

Figure 12 Average friction estimation results.

The creepage – creep force curves for the base, water and oil contamination conditions are shown in Figure 12. The creepage and creep force points have been curve fitted with the Polach creep force model. The identified friction coefficients for these three conditions are: μ_{base}=0.28, μ_{water}=0.08 and μ_{oil}=0.04. The identified μ_0 from curve fitting are close to the results in Figure 11. This good agreement between these two methods proves that the unscented Kalman filter can provide acceptable real time estimation of the wheel – roller friction condition.

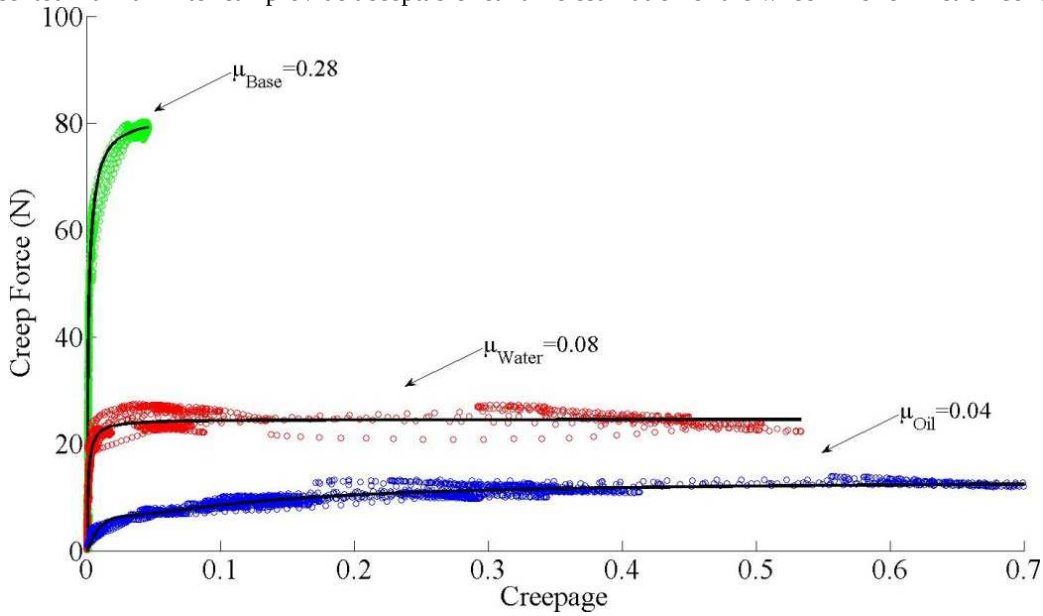

Figure 13 Average friction coefficient

6. CONCLUSIONS AND FUTURE WORK

In this paper, an unscented Kalman filter (UKF) based estimator is developed to monitor the friction coefficient at the wheel – roller interface of a scaled railway roller rig in real time. Measurements without contamination and with applied water and oil have been made to evaluate the performance of the estimator. A large range of creepage is covered by varying the traction load.

The estimator is shown to provide accurate friction estimation under different conditions in real time, but the following problems still remain:

- The estimated friction coefficient is not reliable when the traction load is very small.
- The estimated friction coefficient is also influenced by the traction load but at higher values still remains in an acceptable range.

These problems are most possibly caused by the inaccuracy of the measurements and the system dynamic model. In future work, sensors with better resolution; a high sampling rate of the data acquisition system will be

employed to achieve better estimations. It is also important to develop a better method to tune the UKF, which may also improve the estimation accuracy and stability. Several adaptive tuning algorithms have been proposed and these methods will be studied and employed in the future work.

The roller rig will also be upgraded to carry out more complex experiments. The upgrades include:

- Actuators that can apply different contaminations to the wheel – roller interface in a more controlled manner will be implemented so that the friction condition can be changed during the experiment at a certain time point. In this way, the responding time of the estimator can be evaluated.
- Similarly, better control of the DC generator will be implemented so that the traction load can be changed during the experiment at a certain time point. In this way, the estimator performance under varying traction load can also be studied.

REFERENCES

[1] G. Charles and R. Goodall, "Low Adhesion Estimation," in *The Institution of Engineering and Technology International Conference on Railway Condition Monitoring.*, Birmingham, UK, 2006, pp. 96-101.

[2] C. P. Ward, R. M. Goodall, and R. Dixon, "Creep force estimation at the wheel-rail interface," presented at the 22nd International Symposium on Dynamics of Vehicles on Roads and Tracks (IAVSD2011 Symposium Proceedings), Manchester, UK, 2011.

[3] T. Mei and I. Hussain, "Detection of wheel-rail conditions for improved traction control," in *The 4th International Conference on Railway Traction Systems (RTS2010)*, University of Birmingham, UK 2010, , pp. 1-6.

[4] P. Gáspár, Z. Szabó, and J. Bokor, "Observer based estimation of the wheel-rail friction coefficient," in *IEEE International Conference on Control Applications*, Munich, Germany, 2006, pp. 1043-1048.

[5] M. Covino, M. L. Grassi, and E. Pagano, "Traction electric drives: an indirect identification method of friction forces," in *IEEE International Electric Machines and Drives Conference Record.*, Milwaukee, USA, 1997, pp. TA2/5.1-TA2/5.3.

[6] R. Rizzo and D. Iannuzzi, "Indirect friction force identification for application in traction electric drives," *Mathematics and computers in simulation*, vol. 60, pp. 379-387, 2002.

[7] O. Polach, "A fast wheel-rail forces calculation computer code," *Vehicle System Dynamics*, vol. 33, pp. 728-739, 2000.

[8] Z. Shen, J. Hedrick, and J. E. M. o. T. Design, "A comparison of alternative creep force models for rail vehicle dynamic analysis," *Vehicle System Dynamics*, vol. 12, pp. 79-83, 1983.

[9] M. Lata, "The modern wheelset drive system and possibilities of modelling the torsion dynamics," *Transport*, vol. 23, pp. 172-181, 2008/01/01 2008.

[10] P. Allen and S. D. Iwnicki, "The critical speed of a railway vehicle on a roller rig," *Proceedings of the Institution of Mechanical Engineers, Part F: Journal of Rail and Rapid Transit*, vol. 215, p. 55, 2001.

[11] B. K. Bose, *Modern power electronics and AC drives*: Prentice Hall PTR, 1986.

[12] O. Polach, "Creep forces in simulations of traction vehicles running on adhesion limit," *Wear*, vol. 258, pp. 992-1000, 2005.

[13] J. Kalker, "Wheel-rail rolling contact theory," *Wear*, vol. 144, pp. 243-261, 1991.

[14] S. J. Julier, J. K. Uhlmann, and H. F. Durrant-Whyte, "A new approach for filtering nonlinear systems," in *Proceedings of the American Control Conference*, Seattle, Washington USA, 1995, pp. 1628-1632.

[15] S. J. Julier and J. K. Uhlmann, "Unscented filtering and nonlinear estimation," *Proceedings of the IEEE*, vol. 92, pp. 401-422, 2004.

[16] E. A. Wan and R. van der Merwe, "The unscented Kalman filter for nonlinear estimation," in *Adaptive Systems for Signal Processing, Communications and Control Symposium*, Lake Louise, Alberta, Canada, 2000, pp. 153-158.

[17] L. Jie and Z. Yanru, "Comparison of three Kalman filters for speed estimation of induction machines," in *Industry Applications Conference, Fourtieth IAS Annual Meeting*, Hong Kong, 2005, pp. 1792-1797 Vol. 3.

[18] R. van der Merwe and E. A. Wan, "The square-root unscented Kalman filter for state and parameter-estimation," in *Proceedings of IEEE International Conference on Acoustics, Speech, and Signal Processing (ICASSP '01)*, Salt Lake City, Utah, USA, 2001, pp. 3461-3464 vol.6.